Cell Reports

Report

Tunnel Formation Inferred from the *I*-Form Structures of the Proton-Driven Protein Secretion Motor SecDF

Graphical Abstract

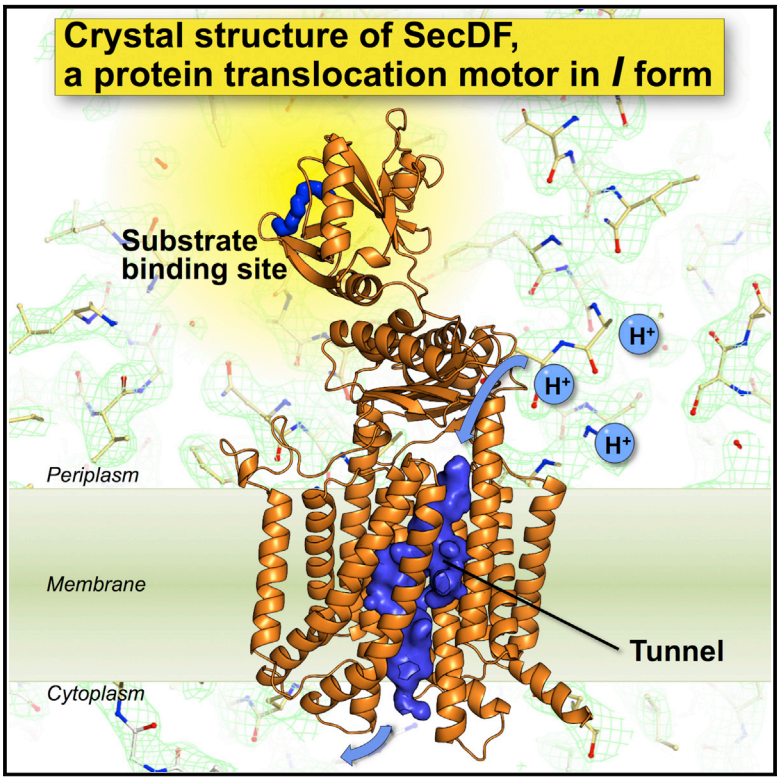

Authors

Arata Furukawa, Kunihito Yoshikaie, Takaharu Mori, ..., Yuji Sugita, Yoshiki Tanaka, Tomoya Tsukazaki

Correspondence

ttsukaza@bs.naist.jp

In Brief

SecDF, a motor protein, uses proton motive force to facilitate bacterial protein translocation mediated by the SecYEG translocon and SecA ATPase. Furukawa et al. describe high-resolution (2.6–2.8 Å) structures of SecDF in *I* forms, providing insight into a substrate binding site and a proton transport pathway through SecDF.

Highlights

- Crystal structures of SecDF in *I* forms are described
- The structures provide insight into an energy-coupling mechanism for Sec machinery
- The structures suggest a substrate binding site and a pathway for protons

Accession Numbers

5XAM
5XAN
5XAP

Furukawa et al., 2017, Cell Reports *19*, 895–901
May 2, 2017
http://dx.doi.org/10.1016/j.celrep.2017.04.030

CellPress

Cell Reports
Report

Tunnel Formation Inferred from the *I*-Form Structures of the Proton-Driven Protein Secretion Motor SecDF

Arata Furukawa,[1] Kunihito Yoshikaie,[1] Takaharu Mori,[2] Hiroyuki Mori,[3] Yusuke V. Morimoto,[4] Yasunori Sugano,[1] Shigehiro Iwaki,[1] Tohru Minamino,[5] Yuji Sugita,[2] Yoshiki Tanaka,[1] and Tomoya Tsukazaki[1,6,*]
[1]Graduate School of Biological Sciences, Nara Institute of Science and Technology, 8916-5 Takayama-cho, Ikoma, Nara 630-0192, Japan
[2]Theoretical Molecular Science Laboratory, RIKEN, 2-1 Hirosawa, Wako-shi, Saitama 351-0198, Japan
[3]Institute for Frontier Life and Medical Sciences, Kyoto University, 53 Shogoin Kawahara-cho, Sakyo-ku, Kyoto 606-8507, Japan
[4]Quantitative Biology Center, RIKEN, 6-2-3 Furuedai, Suita, Osaka 565-0874, Japan
[5]Graduate School of Frontier Biosciences, Osaka University, 1-3 Yamadaoka, Suita, Osaka 565-0871, Japan
[6]Lead Contact
*Correspondence: ttsukaza@bs.naist.jp
http://dx.doi.org/10.1016/j.celrep.2017.04.030

SUMMARY

Protein secretion mediated by SecYEG translocon and SecA ATPase is enhanced by membrane-embedded SecDF by using proton motive force. A previous structural study of SecDF indicated that it comprises 12 transmembrane helices that can conduct protons and three periplasmic domains, which form at least two characterized transition states, termed the *F* and *I* forms. We report the structures of full-length SecDF in *I* form at 2.6- to 2.8-Å resolution. The structures revealed that SecDF in *I* form can generate a tunnel that penetrates the transmembrane region and functions as a proton pathway regulated by a conserved Asp residue of the transmembrane region. In one crystal structure, periplasmic cavity interacts with a molecule, potentially polyethylene glycol, which may mimic a substrate peptide. This study provides structural insights into the Sec protein translocation that allows future analyses to develop a more detailed working model for SecDF.

INTRODUCTION

In bacteria, there are a variety of protein secretion systems, including Sec machinery, the flagellar/type III secretion system, and the TAT (twin arginine translocation) pathway (De Geyter et al., 2016). Among them, protein translocation across the cell membrane via the Sec translocon, SecYEG membrane protein complex, is essential and conserved in all organisms as the Sec pathway (Chatzi et al., 2014; Denks et al., 2014; du Plessis et al., 2011; Rapoport, 2007; Tsirigotaki et al., 2017). In *E. coli*, more than 30% of the newly synthesized proteins are translocated across the cytoplasmic membrane by Sec machinery. Many proteins that have a cleavable signal sequence at the N terminus are generally targeted to the membrane, whereas chaperones such as SecB keep their unfolded states. The following protein translocation is driven by the motor protein SecA ATPase. SecDF has been identified as a secretion factor involved in this protein translocation. SecDF-deficient *E. coli* cells, exhibiting cold sensitivity for growth, are severely defective in protein export at any temperature (Nouwen et al., 2005; Pogliano and Beckwith, 1994). SecDF has been shown to be involved in the later steps of protein translocation (Matsuyama et al., 1993), i.e., protein release from the Sec translocon to the periplasm, using proton motive force across the membrane (Tsukazaki et al., 2011).

In 2011, the first crystal structure of full-length SecDF at 3.3-Å resolution, in the *F* form (retermed the P1-membrane-facing form in this study) (Tsukazaki et al., 2011), revealed that SecDF consists of 12 transmembrane (TM) helices belonging to the RND superfamily (Tseng et al., 1999) as well as three periplasmic domains: P1-head, P1-base, and P4. The TM region is proposed to provide a proton pathway in which a conserved Asp is crucial for proton conduction and proton-driven protein translocation activity. The P1 region interacts with unfolded substrate proteins and probably undergoes functionally coupled conformational transitions between the *F* and *I* forms (retermed P1-intermediate forms in this study). Once SecDF captures a preprotein emerging from SecYEG on the periplasmic side, such repetitive conformational transitions are thought to occur until protein translocation is complete. However, only a predicted structural model of the full-length *I* form is available based on the crystal structure of P1 domain fragment. Furthermore, although SecDF proton-conducting activity was detected (Tsukazaki et al., 2011), the actual proton pathway in the TM region has not yet been structurally identified. Here, we solved the crystal structures of *I* form, one of which shows a plausible tunnel for proton conduction across the membrane. The structures and subsequent functional analyses led to a substantially updated working model of SecDF.

RESULTS AND DISCUSSION

Crystal Structures of SecDF in *I* Form

In the current study, the crystal structures of full-length *I* form were determined using *Deinococcus radiodurans* SecDF 28-760 (DrSecDF) (Figure 1A; Figures S1 and S2; Table S1).

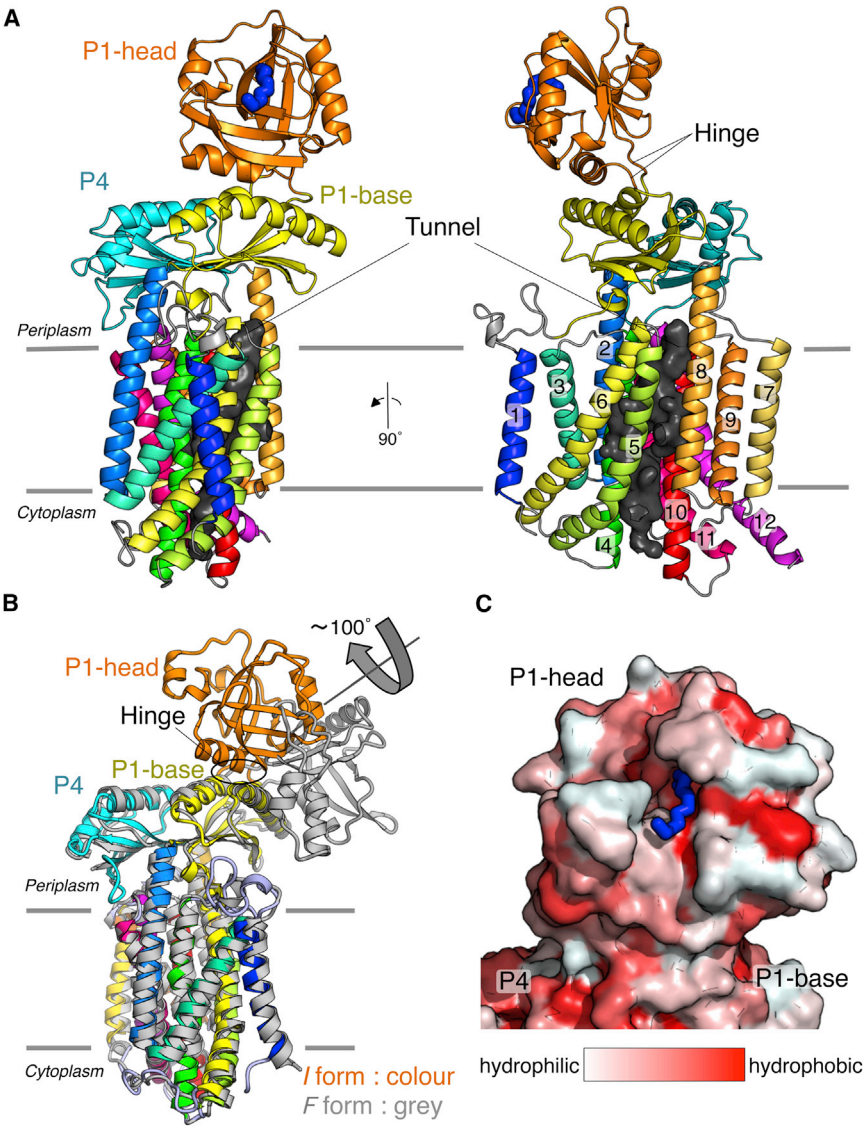

Figure 1. Crystal Structures of SecDF

(A) SecDF in *I* form (MolB). The TM helices are numbered. A part of PEG, O-$(CCO)_4$, in the P1-head cavity is depicted in blue. The tunnel in the TM region is shown as a black surface model.

(B) Structural comparison of the *I* form (MolB, colored as in A) with the *F* form (PDB ID 3AQP, gray).

(C) P1-head in MolB. The PEG molecule is captured by the cavity. The surface model is colored according to hydrophobicity (from white [hydrophilic] to red [hydrophobic]).

See also Figures S1–S3 and Table S1.

The 4.0-Å resolution structure of DrSecDF revealed the overall structure of the *I* form in which the N-terminal regions except for the P1-head (TM1-6 and P1-base) and the C-terminal regions (TM7-12 and P4) are assembled pseudo-symmetrically, similar to those of the previously reported *F* form (Tsukazaki et al., 2011), whereas the P1-head is situated just on the periplasm side of the P1-base (Figure 1; Figure S1). However, this 4.0-Å structure did not further elucidate the function of SecDF. Therefore, to improve the stability of the flexible P1 domain in the crystals, we introduced two cysteine residues at positions 143 and 268, referring to the 4.0-Å structure, to fix the P1-head with higher crystallographic B-factors onto the P1-base by disulfide bond formation (Figure S1A). The mutant SecDF crystals completely formed intramolecular disulfide bonds and diffracted X-rays to over 2.5-Å resolution, enabling us to solve the structures with space groups *C*2 and $P2_12_12_1$ at 2.6- and 2.8-Å resolution, respectively (Table S1; Figure S1). The asymmetric unit of the $P2_12_12_1$ crystal contains two distinct molecules designated MolA and MolB, whereas that of the *C*2 crystal contains one molecule, MolC. In Figure 1A, the crystal structure of MolB is shown as a representative *I* form of SecDF.

As the structures in *I* form did not differ significantly (Figure S1), we hereafter mainly discuss SecDF in *I* form using the higher-resolution MolA-C structures. Each orientation of the P1-head in *I* form as well as in the previously determined P1 domain fragment is structurally distinct (Figure S1), presumably because of its intrinsic flexibility even in *I* form. Superimposition of the *I* (MolB) and *F* forms (PDB ID 3AQP) revealed an approximately 100° rigid-body rotation of the P1-head domain (Figure 1B), with a swinging motion of the P1-head on the P1-base allowed by the two connecting hinge loops.

Interaction Site of Periplasmic Region

Unique features of the MolB crystal structure include an ambiguous electron density at the P1-head cavity, potentially from a part of the polyethylene glycol (PEG) used as a precipitant, whereas there was no electron density map (F_o-F_c) in the same region of the MolA and MolC structures (Figure 1C; Figure S3A). The interaction site in the cavity provides amphipathic surfaces (Figure 1C). The P1-head structure implied that the cavity captures the emerging polypeptide from the SecYEG translocon during protein translocation. We examined this hypothesis using site-directed ultraviolet-cross-linking of pBPA, an ultraviolet-reactive amino acid derivative (Mori and Ito, 2006). pBPA molecules were introduced at each indicated position in the cavity or the exterior periplasmic surface of the *Escherichia coli* SecDF complex (EcSecDF) (Figures S3A and S3B). Following irradiation during protein translocation, ^{35}S-labeled polypeptide cross-linking products were only observed upon introduction of pBPA at position 407, corresponding to Q253 in the DrSecDF cavity (Figures S3C–S3E), suggesting that the P1-head cavity

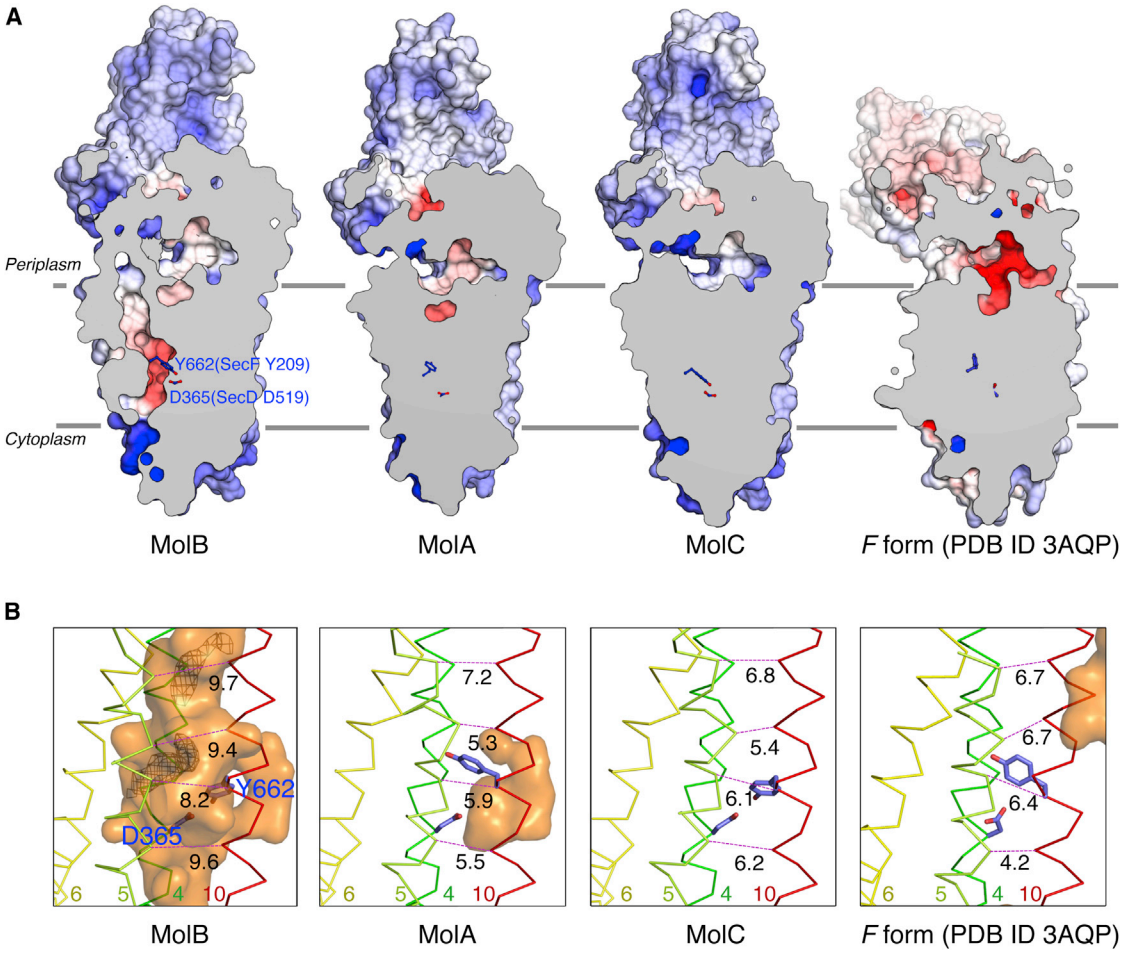

Figure 2. Penetrating Tunnel through the SecDF TM Region

(A) Cut-away models of the surface representations colored as electrostatic potential ranging from blue (+15 kT/e) to red (−15 kT/e). Highly conserved D365 and Y662 residues are shown as blue sticks. The corresponding residues in *E. coli* SecDF are indicated in parentheses.

(B) Close-up view of the middle regions in TM4, 5, 6, and 10. The spaces in the TM region are depicted as an orange surface model with 40% transparency. Cα-Cα distances (in angstroms) between TM5 and TM10 are shown. The F_o-F_c electron density map (2.0 σ) in the tunnel is shown as mesh.

See also Figure S4.

provides interaction sites for the newly synthesized polypeptide. Whereas the *I*-form P1 cavities in MolA, B, C, and the P1 domain fragment possess sufficient room for the molecule binding, the *F*-form cavity size is reduced (Figures S4A–S4E). Thus, the *I* form likely holds substrates more stably than the *F* form, which may be closely related to the dynamic catch and release of the substrate on the periplasmic side during protein translocation.

Tunnel Architecture in TM Region

Additionally, MolB exhibits a partially hydrophilic, penetrated tunnel through its TM region not observed in the other SecDF *I*-form or *F*-form structures (Figures 1A and 2), in large part owing to an approximately 4-Å shift of TM5 toward the outside compared to that of MolA, MolC, and the *F*-form structure (Figure 2B; Figures S4F–S4I and S5A). In fact, the root-mean-square deviations (RMSDs) of TM5 showed higher values than those of other TMs (Figure S1E). A negative electrostatic potential exists at the tunnel center arising from Asp (D365), an essential, highly conserved residue for SecDF protein translocation activity and proton transport (Tsukazaki et al., 2011). The conserved Y662 residue can associate with D365 by hydrogen bonding and possesses the only fluctuating aromatic side chain in TMs in *I*-form structures (Figures 2A and 2B; Figures S4F–S4I). Mutational analyses of growth complementation, protein translocation activities, and proton conductance confirmed the importance of Y662 (Figures S5F and S6B).

The crystal structures of SecDF in *I* form identified over ten water molecules in the TM region on the cytoplasmic side, implying their accessibility to the vicinity of D365 from the cytoplasm but not from the periplasm. Unidentified electron densities within the MolB tunnel may also be due to small molecules such as water (Figure 2B). To elucidate the tunnel formation mechanism, we performed all-atom molecular-dynamics (MD)

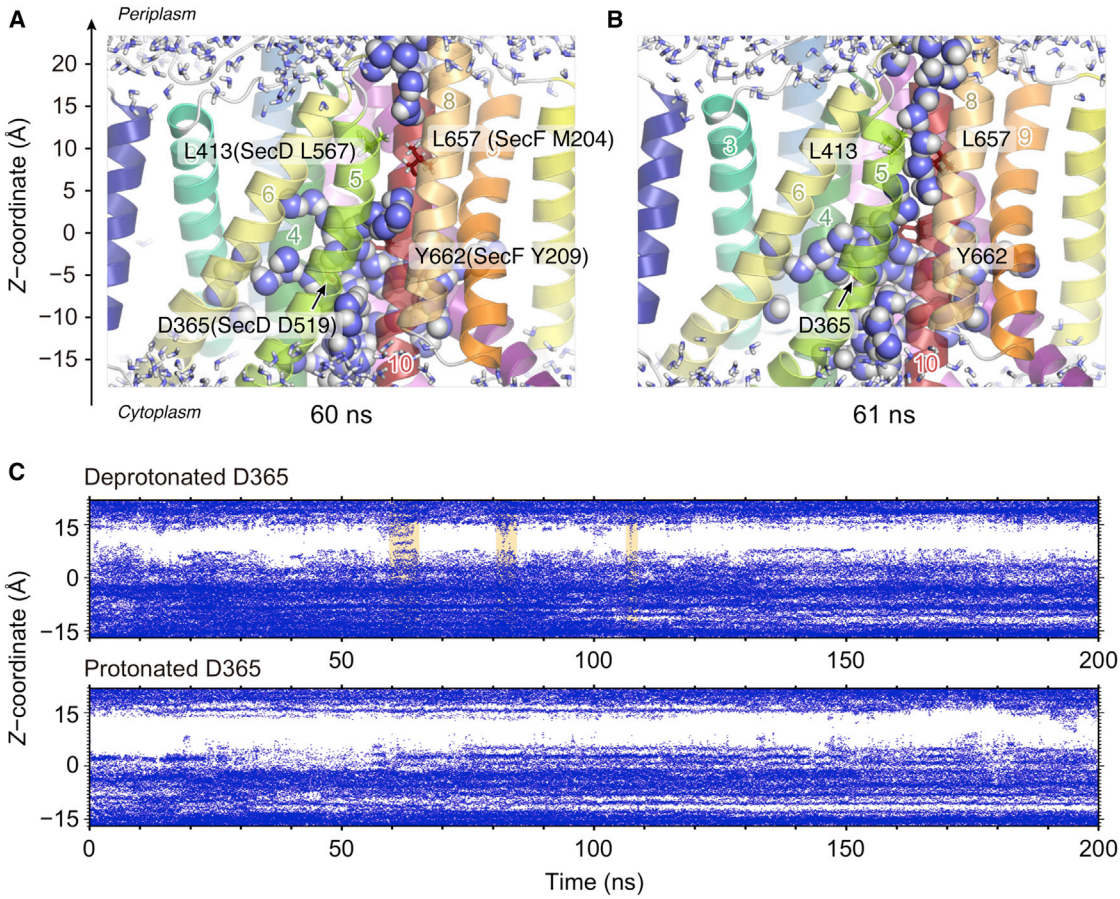

Figure 3. Hydrogen-Bonded Water Molecules along the Tunnel

(A and B) Snapshots of SecDF at 60 ns (A) and 61 ns (B) in the MD simulation when D365 was deprotonated. Some water molecules in the TM region at 61 ns formed a hydrogen-bonded single-file chain along the tunnel.

(C) Time courses of *z* coordinates of water oxygen in the TM region in the MD simulation of deprotonated and protonated D365. Yellow shading indicates the periods wherein the water chain was created.

See also Figure S5 and Movie S1.

simulations of SecDF using the highest-resolution structure MolC, which does not have the tunnel architecture, as the initial conformation. The mutation residues I143C and L268C in MolC were reverted to the wild-type residues. For MD simulation, the SecDF model was equilibrated in phosphatidyl ethanolamine (POPE). Then, we examined the effect of the protonation state of D365, which has been predicted to have unusual pKa (7.5–8.5) by PROPKA and MCCE (Li et al., 2005; Song et al., 2009), on SecDF structural change. D365 deprotonation attracted water molecules from the cytoplasmic bulk phase, leading to an outward TM5 shift (approximately 2.4 Å) to form a tunnel as revealed in MolB; the significant shift was not observed when D365 was protonated (Figures S5A–S5C). Simulations with the deprotonated also demonstrated repeated single-file hydrogen-bonded water chain formation (Figure 3) along the vicinity of the MolB crystal structure tunnel position. Rapid growth occurred from both the cytoplasmic and periplasmic sides (Movie S1). Specifically, D365 deprotonation might reduce the large free-energy barrier (z = 5–12 Å) on the hydrophobic periplasmic side of the TM region as indicated by water molecule distribution, such that the hydrophobic side-chain fluctuations of L413 and L657 induce water chain formation. Additionally, simulations indicated Y662 side-chain conformational transition between two orientations, as observed in the MolA and MolB/MolC crystal structures (Figure 2B; Figure S5G). Y662F mutant showed minimal growth complementation ability but exhibited similar translocation activity as the control. These differences may be attributable to the varying culture conditions (Figure S5F). As observed for the various Y209 mutants, the Y662F mutant could exhibit minimal SecDF activity, suggesting that the bulky aromatic side chain is essential for providing sufficient space for tunnel formation. As D365 is critical for proton conductance (Tsukazaki et al., 2011) (Figure S6B), we therefore propose that the tunnel in the *I* form (MolB) reflects the proton pathway in SecDF by means of a water chain generated through D365 deprotonation, wherein the proton hops between hydrogen-bonded water molecules via the Grotthuss mechanism.

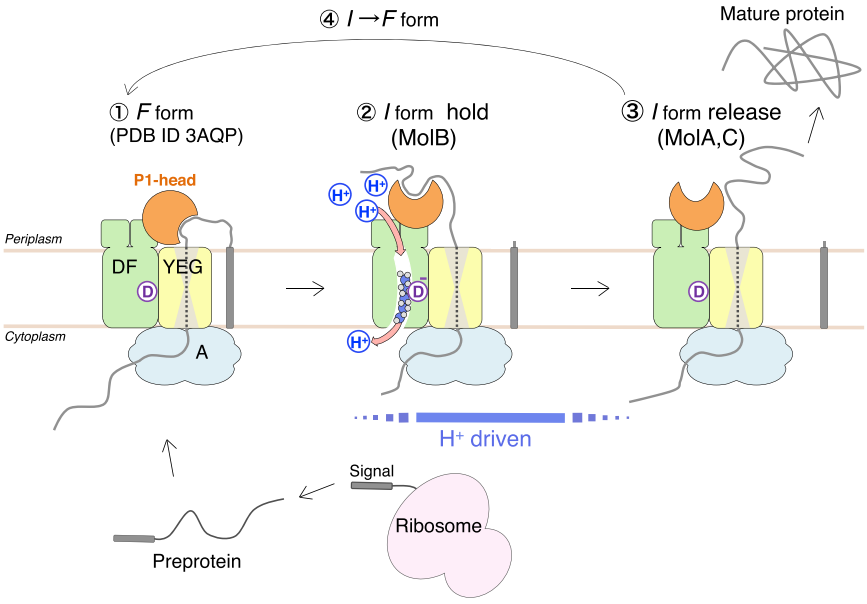

Figure 4. Working Model of Proton-Driven Protein Translocation by SecDF

Translated preproteins with an N-terminal signal sequence are targeted and inserted into the Sec machinery. SecDF interacts with the preprotein on the periplasmic side and drives protein translocation via P1-head domain transitions. The conserved essential Asp is circled. 1, SecDF *F* form (PDB ID 3AQP), capturing state. The signal peptide is cleaved during protein translocation. 2, *I* form, holding state (MolB). The protons are transported via water molecules, shown in blue and white, through the open tunnel. 3, *I* form, releasing state (MolA or MolC). The tunnel is closed. 4, Transition from *I* to *F* form.
See also Figure S6.

Functional Flexibility of SecDF

In vivo proton transport analysis using a pH indicator (Morimoto et al., 2010, 2011) demonstrated that P1-head flexibility is closely related to proton permeation (Figures S6A–S6C). However, MD simulations showed that tunnel formation in the D365 deprotonation condition was not accompanied by significant periplasmic domain conformational transition, perhaps owing to the lack of systemic proton flow (Movie S1). Conversely, transduction of the conformational changes between the TM region and the P1-head arising from proton permeation should alter the configuration of the sandwiched P4 and P1-base region (Figure S6D). To confirm that this dynamic structural alternation is required for SecDF activity, we performed complementation tests and a protein translocation assay using another double-cysteine mutant of SecDF (Figures S6D–S6F). Inhibition of SecDF activity following SecDF disulfide bond-mediated P4 and P1-base fixation was reversed by the reductant DTT, indicating that P1-base and P4 domain flexibility is also crucial. Thus, the SecDF domains all appear to undergo precisely organized, dynamic conformational changes in response to proton transport.

Working Model for SecDF

We propose the following plausible working model for SecDF (Figure 4), although further structural and functional analyses are required to fully understand the SecDF mechanism. Presecretory proteins are synthesized by ribosomes and post-translationally targeted to the translocon prior to translocation across the membrane. Initially, SecA ATPase repeatedly pushes the preprotein into the SecYEG. SecDF in the *F* form then interacts with the emergent preprotein on the periplasmic side and the P1-head conformation changes from the *F* to the *I* form accompanied with preprotein dragging. The MolB structure may represent a snapshot in which the preprotein is captured and extended into the periplasmic space by the P1 domain. The MolB structure shows the tunnel architecture in the TM region but does not contain the chained water molecules along the tunnel (Figure 2B). Because of the elevated SecDF proton transport activity observed in the presence of an unfolded protein on the periplasmic side (Tsukazaki et al., 2011), the MolB state would undergo further structural changes to form the transient proton transport pathway. Deprotonation of the conserved Asp at the center of the pathway may release protons in the cytoplasm and trigger opening of the proton pathway. In conjunction with proton conduction from the periplasm to cytoplasm, SecDF may release substrate proteins into the periplasmic space. After preprotein release, the tunnel may close as represented by MolA and MolC followed by a conformational change from the *I* to the *F* form. These dynamic transition cycles may repeat until the secretory protein is completely translocated. Notably, a SecDF paralog present in some bacteria such as *Vibrio alginolyticus* incorporates a sodium ion rather than a proton gradient (Ishii et al., 2015), probably through a similar penetrating tunnel of equivalent origin, which would be sufficiently large to allow influx of sodium ions via the TM region. However, the ion selectivity of SecDF remains unclear.

EXPERIMENTAL PROCEDURES

Purification and Crystallization of SecDF

The gene encoding DrSecDF(Met-28-768)-His_8 registered in NCBI Reference Sequence (WP_010888457.1) was inserted into pTV118N (Takara), and the recombinant plasmid was introduced into *E. coli* strain BL21(DE3). The procedures from cell culture to Ni-NTA column chromatography were as described previously (Tsukazaki et al., 2006). Column fractions were concentrated using an Amicon Ultra (50-kDa cutoff; Merck Millipore) and loaded on a Superdex 200 16/600 (GE Healthcare) in 20 mM Tris-HCl, pH 8.0, 300 mM NaCl, 0.1 mM 4-(2-aminoethyl) benzenesulfonyl fluoride hydrochloride, and 0.1% *n*-dodecyl-beta-D-maltoside (DDM). SecDF was concentrated to about 20 mg/mL and crystallized using a Gryphon LCP (Art Robbins Instruments) (Kumazaki et al., 2014). SecDF crystals were grown at 20°C in a reservoir solution containing 38% PEG200, 100 mM Na-citrate, pH 5.9, and 100 mM NH_4-citrate in 7 days.

The SecDF mutants were prepared and crystallized by the same procedures. The *C*2 and $P2_12_12_1$ crystals of DrSecDF(I143C, L268C) were grown in reservoir solutions of (41% PEG200, 100 mM Na-citrate, pH 5.9, and

100 mM NH_4NO_3) and (40% PEG200, 100 mM Na-citrate, pH 6.6, and 100 mM $LiSO_4$), respectively.

Data Collection and Structure Determination

The X-ray diffraction data were collected at SPring-8 beamline BL32XU. Initial phases were calculated by molecular replacement with the SecDF structure (PDB ID 3AQP), except for the flexible P1-head, using PHASER (McCoy et al., 2007). The model was rebuilt manually using COOT (Emsley and Cowtan, 2004) and refined using PHENIX (Adams et al., 2010). Molecular graphics were generated with PyMol (Schrödinger) and CueMol2 (http://www.cuemol.org/).

Complementation Tests and Translocation Assay of *E. coli* SecD and SecF Mutants

The *secD1*(Cs) transformants, carrying pFLAG-CTC and a plasmid encoding hemagglutinin (HA)-tagged *E. coli* SecD/SecF mutant, were prepared as described previously (Tsukazaki et al., 2011). For growth tests, the *secD1*(Cs) cells were spotted onto Luria-Bertani (LB)-agar plates and incubated at 20°C for 48 hr. To check SecDF accumulation, the cells were grown in LB medium at 20°C for 12 hr. The accumulation of SecDF was confirmed by immunoblotting (Tsukazaki et al., 2011). In vivo translocation assay was performed as described previously (Tsukazaki et al., 2011). Disulfide bond formation of EcSecD(R439C)F(E132C) was induced by diamide (Tsukazaki et al., 2011).

In Vitro Photo-Cross-Linking with Preprotein

E. coli secD1(Cs) was transformed with pHM649 encoding the pBPA-incorporating system (Mori and Ito, 2006) and a *secD-secF* plasmid with an engineered amber codon in *secD*. Cells were grown in LB medium containing 0.1 mM pBPA until mid-log phase, and production of SecD(pBPA) was then induced for 1 hr at 37°C with 0.2% arabinose. Inverted membrane vesicles (IMVs) were prepared and used to generate the ^{35}S-proOmpA(L59) translocation intermediate in a standard translocation reaction with 5 mM ATP and 5 mM succinate (Tsukazaki et al., 2011; Uchida et al., 1995). Samples were mixed with an equal volume of 50 mM HEPES-KOH (pH 7.5)-5 mM $MgSO_4$ and incubated at 37°C for 60 min. For detection of translocation intermediates, samples were treated with 0.6 mg/mL proteinase K at 0°C for 20 min and precipitated with 5% trichloroacetic acid (TCA). They were analyzed by SDS-PAGE and phosphor imaging. For interaction analysis, samples were either directly precipitated with 5% TCA or irradiated with UV at 4°C for 20 min using a B-100AP UV lamp (Ultraviolet Products) at a distance of 4 cm. They were analyzed by SDS-PAGE and phosphor imaging, either directly or following immunoprecipitation with anti-SecD.

Intracellular pH Measurement

The *E. coli* BL21(DE3) was transformed with the D*rsecDF*-encoding plasmid and pYVM063, which encodes the ratiometric pH indicator protein pHluorin(M153R) (Morimoto et al., 2011). The transformants were grown in LB containing 1 mM isopropyl β-D-1-thiogalactopyranoside (IPTG) and 0.2% arabinose at 30°C for 8 hr. To reduce disulfide crosslinking, 5 mM DTT was added. The fluorescence spectra were measured using a fluorescence spectrophotometer (RF-5300PC; Shimadzu). Intracellular pH was determined from a pH-dependent calibration curve generated by the 410/470-nm excitation ratios of purified pHluorin(M153R).

All-Atom MD Simulation of SecDF in a POPE Lipid Bilayer

We examined the effect of the protonation state of D365 on the conformational change of SecDF by using all-atom MD simulations with GENESIS (Jung et al., 2015). We modeled two systems ($D365^H$ and $D365^-$), where D365 is protonated in $D365^H$ and deprotonated in $D365^-$. The protonation states of the other acidic and basic residues were predicted with reference to pKa values calculated by PROPKA and MCCE (Li et al., 2005; Song et al., 2009). The X-ray crystal structure of the *I*-form SecDF (MolC) was embedded in a POPE lipid bilayer and solvated with 150 mM KCl salt solution. The mutation sites, I143C and L268C, in MolC were altered to the wild-type residues. We performed 200-ns MD simulations in the *NPT* ensemble at T = 300 K and P = 1 atm. The protocols and algorithms used in the MD simulations were the same as those in our previous study on SecYEG (Tanaka et al., 2015).

ACCESSION NUMBERS

The accession numbers for the atomic coordinates of SecDF reported in this paper are PDB: 5XAM, 5XAN, and 5XAP.

SUPPLEMENTAL INFORMATION

Supplemental Information includes six figures, one table, and one movie and can be found with this article online at http://dx.doi.org/10.1016/j.celrep.2017.04.030.

AUTHOR CONTRIBUTIONS

Conceptualization, T.T.; Methodology and Investigation, A.F., K.Y., T.M., H.M., Y.V.M., Y. Sugano, S.I., T.M., Y. Sugita, Y.T., and T.T.; Writing, A.F. and T.T.; Supervision, T.T.

ACKNOWLEDGMENTS

We thank K. Kobayashi for technical support; K. Abe for secretarial assistance; H. Konno, T. Haruyama, R. Watanabe, and N. Soga for useful discussion; and the beamline scientists at BL32XU of SPring-8 (Hyogo, Japan) for help with data collection. The synchrotron radiation experiments were performed at BL32XU of SPring-8 with the approval of the Japan Synchrotron Radiation Research Institute (JASRI) (Proposals 2016A2532, 2015B2061, 2015A1061, and 2014B1109). The MD simulations were performed on TSUBAME2.5 at the Tokyo Institute of Technology through the HPCI System Research Project (Project ID hp160184) and on HOKUSAI GreatWave at RIKEN. This work was supported by JSPS/MEXT KAKENHI Grants JP26119006, JP26119007, JP26291023, JP24117003, JP24117004, JP16K14713, JP15H01335, JP15H01537, JP15H01640, JP15H05594, JP15J08235, JP15K06972, and JP15K14490; by the Mitsubishi Foundation; by the Noguchi Institute; by the Naito Foundation; by the Mochida Memorial Foundation for Medical and Pharmaceutical Research; and by PRESTO, JST (Grant JPMJPR12L3).

Received: February 13, 2017
Revised: March 16, 2017
Accepted: April 11, 2017
Published: May 2, 2017

REFERENCES

Adams, P.D., Afonine, P.V., Bunkóczi, G., Chen, V.B., Davis, I.W., Echols, N., Headd, J.J., Hung, L.W., Kapral, G.J., Grosse-Kunstleve, R.W., et al. (2010). PHENIX: a comprehensive Python-based system for macromolecular structure solution. Acta Crystallogr. D Biol. Crystallogr. *66*, 213–221.

Chatzi, K.E., Sardis, M.F., Economou, A., and Karamanou, S. (2014). SecA-mediated targeting and translocation of secretory proteins. Biochim. Biophys. Acta *1843*, 1466–1474.

De Geyter, J., Tsirigotaki, A., Orfanoudaki, G., Zorzini, V., Economou, A., and Karamanou, S. (2016). Protein folding in the cell envelope of Escherichia coli. Nat. Microbiol. *1*, 16107.

Denks, K., Vogt, A., Sachelaru, I., Petriman, N.A., Kudva, R., and Koch, H.G. (2014). The Sec translocon mediated protein transport in prokaryotes and eukaryotes. Mol. Membr. Biol. *31*, 58–84.

du Plessis, D.J., Nouwen, N., and Driessen, A.J. (2011). The Sec translocase. Biochim. Biophys. Acta *1808*, 851–865.

Emsley, P., and Cowtan, K. (2004). Coot: model-building tools for molecular graphics. Acta Crystallogr. D Biol. Crystallogr. *60*, 2126–2132.

Ishii, E., Chiba, S., Hashimoto, N., Kojima, S., Homma, M., Ito, K., Akiyama, Y., and Mori, H. (2015). Nascent chain-monitored remodeling of the Sec machinery for salinity adaptation of marine bacteria. Proc. Natl. Acad. Sci. USA *112*, E5513–E5522.

Jung, J., Mori, T., Kobayashi, C., Matsunaga, Y., Yoda, T., Feig, M., and Sugita, Y. (2015). GENESIS: a hybrid-parallel and multi-scale molecular dynamics simulator with enhanced sampling algorithms for biomolecular and cellular simulations. Wiley Interdiscip. Rev. Comput. Mol. Sci. *5*, 310–323.

Kumazaki, K., Tsukazaki, T., Nishizawa, T., Tanaka, Y., Kato, H.E., Nakada-Nakura, Y., Hirata, K., Mori, Y., Suga, H., Dohmae, N., et al. (2014). Crystallization and preliminary X-ray diffraction analysis of YidC, a membrane-protein chaperone and insertase from Bacillus halodurans. Acta Crystallogr. F Struct. Biol. Commun. *70*, 1056–1060.

Li, H., Robertson, A.D., and Jensen, J.H. (2005). Very fast empirical prediction and rationalization of protein pKa values. Proteins *61*, 704–721.

Matsuyama, S., Fujita, Y., and Mizushima, S. (1993). SecD is involved in the release of translocated secretory proteins from the cytoplasmic membrane of *Escherichia coli*. EMBO J. *12*, 265–270.

McCoy, A.J., Grosse-Kunstleve, R.W., Adams, P.D., Winn, M.D., Storoni, L.C., and Read, R.J. (2007). Phaser crystallographic software. J. Appl. Cryst. *40*, 658–674.

Mori, H., and Ito, K. (2006). Different modes of SecY-SecA interactions revealed by site-directed in vivo photo-cross-linking. Proc. Natl. Acad. Sci. USA *103*, 16159–16164.

Morimoto, Y.V., Che, Y.S., Minamino, T., and Namba, K. (2010). Proton-conductivity assay of plugged and unplugged MotA/B proton channel by cytoplasmic pHluorin expressed in Salmonella. FEBS Lett. *584*, 1268–1272.

Morimoto, Y.V., Kojima, S., Namba, K., and Minamino, T. (2011). M153R mutation in a pH-sensitive green fluorescent protein stabilizes its fusion proteins. PLoS One *6*, e19598.

Nouwen, N., Piwowarek, M., Berrelkamp, G., and Driessen, A.J. (2005). The large first periplasmic loop of SecD and SecF plays an important role in SecDF functioning. J. Bacteriol. *187*, 5857–5860.

Pogliano, J.A., and Beckwith, J. (1994). SecD and SecF facilitate protein export in *Escherichia coli*. EMBO J. *13*, 554–561.

Rapoport, T.A. (2007). Protein translocation across the eukaryotic endoplasmic reticulum and bacterial plasma membranes. Nature *450*, 663–669.

Song, Y., Mao, J., and Gunner, M.R. (2009). MCCE2: improving protein pKa calculations with extensive side chain rotamer sampling. J. Comput. Chem. *30*, 2231–2247.

Tanaka, Y., Sugano, Y., Takemoto, M., Mori, T., Furukawa, A., Kusakizako, T., Kumazaki, K., Kashima, A., Ishitani, R., Sugita, Y., et al. (2015). Crystal Structures of SecYEG in Lipidic Cubic Phase Elucidate a Precise Resting and a Peptide-Bound State. Cell Rep. *13*, 1561–1568.

Tseng, T.T., Gratwick, K.S., Kollman, J., Park, D., Nies, D.H., Goffeau, A., and Saier, M.H., Jr. (1999). The RND permease superfamily: an ancient, ubiquitous and diverse family that includes human disease and development proteins. J. Mol. Microbiol. Biotechnol. *1*, 107–125.

Tsirigotaki, A., De Geyter, J., Šoštaric, N., Economou, A., and Karamanou, S. (2017). Protein export through the bacterial Sec pathway. Nat. Rev. Microbiol. *15*, 21–36.

Tsukazaki, T., Mori, H., Fukai, S., Numata, T., Perederina, A., Adachi, H., Matsumura, H., Takano, K., Murakami, S., Inoue, T., et al. (2006). Purification, crystallization and preliminary X-ray diffraction of SecDF, a translocon-associated membrane protein, from *Thermus thermophilus*. Acta Crystallogr. Sect. F Struct. Biol. Cryst. Commun. *62*, 376–380.

Tsukazaki, T., Mori, H., Echizen, Y., Ishitani, R., Fukai, S., Tanaka, T., Perederina, A., Vassylyev, D.G., Kohno, T., Maturana, A.D., et al. (2011). Structure and function of a membrane component SecDF that enhances protein export. Nature *474*, 235–238.

Uchida, K., Mori, H., and Mizushima, S. (1995). Stepwise movement of preproteins in the process of translocation across the cytoplasmic membrane of *Escherichia coli*. J. Biol. Chem. *270*, 30862–30868.